Research Article

Electrochemical Characterization of Thin Film/Nanodots Electrodes of Silver and Gold for Biosensing CCRF-CEM Leukemia Cells

Ulya Farahdina, Miftakhul Firdhaus, Putri Wulandari, Agus Rubiyanto and Nasori Nasori*
Laboratory Medical Physics and Biophysics, Department of Physics, Faculty of Sciences and Data Analytic, Institut Teknologi Sepuluh Nopember, Surabaya, Indonesia

Ihwanul Aziz
Research Center for Accelerator Technology, Research Organization of Nuclear Energy, National Research and Innovation Agency (BRIN), Yogyakarta, Indonesia

Hari Suprihatin
Directorate of Laboratory Management, Research Facilities, and Science and Technology Park, National Research and Innovation Agency (BRIN), Yogyakarta, Indonesia

Nurul Jadid
Department of Biology, Institut Teknologi Sepuluh Nopember (ITS), Surabaya, Indonesia

Rini Khamimatul Ula
Research Center for Electronic, National Research and Innovation Agency of Indonesia (BRIN), Jakarta, Indonesia

* Corresponding author. E-mail: nat.nasori@its.ac.id DOI: 10.14416/j.asep.2024.09.003
Received: 14 May 2024; Revised: 24 June 2024; Accepted: 31 July 2024; Published online: 4 September 2024

Abstract
This study presents a novel biosensor for detecting CCRF-CEM cells, derived from a T lymphoblastoid cell line, featuring intricate surface modification techniques. The fabrication process involves thin film deposition, electropolishing and dual anodization to create an anodic aluminum oxide template, followed by DC sputtering deposition to produce gold (Au) thin film/silver (Ag) nanodots and an Ag thin film/Au nanodots electrodes. Characterization using scanning electron microscopes (SEM), energy-dispersive X-ray spectroscopy (EDX), and X-ray diffraction (XRD) confirms electrode suitability for biosensing applications. Surface modification with aptamer Sgc8c and bovine serum albumin enables specific binding of CCRF-CEM cells while minimizing non-specific interactions. Electrochemical characterization via cyclic voltammetry (CV) and electrochemical impedance spectroscopy (EIS) reveals the biosensor's sensitivity, selectivity, and reproducibility. The Au thin film/Ag nanodots electrode emerges as the most promising choice, exhibiting exceptional sensitivity (limit of detection (LOD) = 16 cell/10 mL), reproducibility, and selectivity for CCRF-CEM cells. This work highlights the importance of tailored surface development in biosensor design and lays the groundwork for highly sensitive and selective biosensors with potential applications in disease diagnosis and therapeutic monitoring.

Keywords: Biosensor, CCRF-CEM, Electrochemical characterization, Fabrication, Thin film/nanodots electrode

1 Introduction

The spread of cancer cells to other body tissues is known as metastasis. In this condition, the cancer is already in an advanced stage or difficult to treat. Metastatic cancer can spread to the bloodstream and spinal cord [1]. In 2023, It was recorded that blood cancer sufferers will be the fifth type of cancer with

the highest number of sufferers in the world with an increase in the number of sufferers of more than 1,958,310 people compared to the previous year [2], [3]. This type of cancer can usually be diagnosed when it has metastasized. Thus, blood cancer ranks 9th in the type of cancer that has the lowest life expectancy, namely 70% in a 5-year period [4].

Blood cancer is classified into acute lymphocytic leukemia (ALL), acute myeloid leukemia (AML), chronic lymphocytic leukemia (CLL), chronic myeloid leukemia (CML), and hairy cell leukemia (HCL). This classification is based on the type of genetic mutation that occurs in the chromosome and results in different expressions in white blood cells [5]. The most common cancer in children is ALL type blood cancer with a fairly large increase in the number of sufferers every year [6]. This blood cancer is caused by a deletion mutation in the IKZF1 gene resulting in the formation of excess blood cells, which can eat healthy blood cells [7]. Early identification and targeted treatment are crucial for improving the life expectancy of individuals with ALL, as it is characterized by swift disease propagation [8].

Immunosensors can be used to detect a disease through precise biomolecule-cell interactions, especially in leukemia. The biomarker and bioreceptor components that can be used for the development of biosensors include CCRF-CEM cells, Molt-4 cells, and anti-CD5 antibodies for ALL; HL60 and KG1a cell lines, CD123 antibodies, and FLT3 gene probes for AML; as well as ZAP70 gene probes, BCR/ABL fusion gene probes, and aptamers for CLL and CML [9]. Electrochemical biosensors offer high sensitivity, rapid detection, multiplexing, and cost-effectiveness [10]. In ALL detection, exceptional sensitivity arises from specific bioreceptors targeting leukemia cells, advanced nanomaterials like gold nanoparticles and quantum dots amplifying signals, and cutting-edge electrochemical techniques like cyclic voltammetry (CV), electrochemical impedance spectroscopy (EIS), and differential pulse voltammetry (DPV) ensuring precise quantification [11]–[13]. These advancements underscore the pivotal role of immunosensors in revolutionizing leukemia diagnostics, promising enhanced precision and efficacy in disease management.

Exploring biosensor design, particularly integrating gold and silver components, reveals their significant impact, attributed to their stability and conductivity. Gold offers strong biomolecule binding such as protein, while silver facilitates efficient electron transfer, unveiling cellular interactions [14]–[18]. In this work, we developed thin films decorated with Ag- and Au-based nanodots to create surfaces conducive to binding a broader spectrum of biomarkers. Through this approach, we devised a modified electrochemical aptasensor for precise, sensitive, and early detection of ALL type blood cancer cells, particularly CCRF-CEM cells. This electrochemical biosensor, characterized by its sensitivity, cost-effectiveness, and accuracy, was meticulously crafted with Ag serving as a signal amplification label and Au functioning as a bioreceptor binding electrode, boasting exceptional biocompatibility.

2 Materials and Methods

2.1 *Materials*

The chemicals used in the study include sodium hydroxide (NaOH), phosphoric acid (H_3PO_4), copper(II) chloride ($CuCl_2$), acetone (C_3H_6O), oxalic acid ($(CH_2OH)_2$), ethanol (C_2H_5OH), chromic acid (CH_2CrO_4), Poly(methyl methacrylate) (PMMA), potassium ferrocyanide ($K_4[Fe(CN)_6].3H_2O$), hydrochloric acid (HCl), and deionized (DI) water, all obtained from Sigma Aldrich. Additionally, thick aluminum foil, silver, and gold were procured from Advance Tapes and Goodfellow. Indium tin oxide (ITO) glass was obtained from Ali Laboratory and Mechanics (Surabaya, Indonesia). Other materials, including phosphate buffer saline (PBS), sgc8c, CCRF-CEM cell line, RPMI 1640, Glutamine, Foetal Bovine Serum (FBS), and bovine serum albumin (BSA), were also purchased from Sigma Aldrich, Singapore.

2.2 *Fabrication of AAO*

The fabrication of Anodized Aluminum Oxide (AAO) involved several steps, including electropolishing, two-stage anodization, oxide removal, and pore widening. Electropolishing was carried out using a solution of 60% $HClO_4$ + ethanol (1:7, v/v) at 0 °C with a voltage of 20 V for 2.5 minutes to level the surface. This was followed by the first anodization in a solution of 3 M $(CH_2OH)_2$ at 80 °C at 40 V for 8 h to form pores. Subsequently, oxide removal was performed by immersing aluminum in a solution of 6 wt% H_3PO_4 + 1.5 wt% H_2CrO_4 at room temperature for 13 h. The second anodization was conducted using a solution of 3 M $(CH_2OH)_2$ at 80 °C at 40 V for 10 min to make the pores arranged more neatly. Chemical pore widening was then carried out using a 5% phosphoric acid solution.

2.3 *Fabrication of nanodots and thin film electrodes*

The fabrication of nanodots and thin film electrodes was achieved through DC sputtering deposition at BRIN Yogyakarta, Indonesia. This DC sputtering deposition method is carried out with sputtering targets in the form of Ag and Au. The process of thin film fabrication involved placing sputtering targets at a distance of 25 mm from the substrate and adjusting the base pressure of the DC sputtering tube to 10^{-2} Pa, pure argon gas (99.99%) at a constant pressure of 60 Pa, the voltage applied between the cathode (sputtering target) and anode (substrate) of 1 kV, with a deposition duration of 30 seconds. After deposition, the AAO coating will be transformed into ultra-thin alumina masks (UTAMs) to enable adhesion to thin films. The transformation of AAO into UTAMs is achieved by immersing AAO transformed into UTAMs in a saturated $CuCl_2$ solution. Subsequently, UTAMs are immersed in a mixture of $CuCl_2$ solution (85 wt%) and HCl (15 wt%) for 10 min. UTAMs are then placed on the conductive Indium Tin Oxide (ITO) glass layer with the aid of a plastic sieve. Nanodots on top of UTAMs will be deposited using the same parameter of the DC sputtering method as the thin film deposition. Then, UTAMs are cleaned with adhesive tape that is peeled off.

2.4 *Cell culture*

CCRF-CEM cells (the peripheral blood of a 4-year-old female Caucasian with acute lymphoblastic leukemia (ALL)) were cultured by thawing in a cell culture medium at 37 °C. Subsequently, the outer surface of the cell culture flask was wiped with 70% ethanol, then its contents were transferred to a 15 mL centrifuge tube and centrifuged at 251.55 xRCF for 3 min. Then, the cells were resuspended in 10 mL of growth media and transferred to a cell culture flask. The cells were incubated at 5% CO_2, 37 °C in a humidified incubator. Following the cell culture step, CCRF-CEM cells at a specific concentration were added onto nanodots and incubated at 37 °C for 2 h. Afterwards, the electrodes were immersed in PBS (0.01 M, pH 7.4) to remove unbound cells. The concentration of CCRF-CEM cells used ranged from 10^2 to 10^6 cells/mL.

2.5 *Surface modification*

Surface modification was performed by pipetting 10 µL of aptamer with a concentration of 1 mg/mL onto the electrode surface. Subsequently, the electrode was incubated at 37 °C for 2 h to produce Thin film/nanodots/aptamer complexes. Afterwards, the electrode was rinsed with 0.01 M PBS (pH 7.4) to remove unbound aptamers. Next, the electrode was immersed in 10 µL of 0.01 M PBS containing 0.5% BSA for 10 min to block remaining active sites and eliminate non-specific binding effects. Then, thorough washing with 0.01 M PBS was conducted. The thin film/nanodots/aptamer/BSA biosensor was stored at 4 °C. Two hours before blood cancer detection electrode performance testing, cell deposition was performed on the electrode.

2.6 *Characterization and electrochemical measurements*

X-ray diffraction (XRD) analysis was conducted using an X'pert Pro X-ray Diffraction instrument (Germany). Morphological structures of the nanodots and thin films were identified using a Phenom scanning electron microscope and energy-dispersive X-ray spectroscopy (EDS) equipped with a Thermo Scientific ProX-G6 (Institut Teknologi Sepuluh Nopember, Indonesia). Electrode performance for cell detection was assessed using a CorrTest CS2350 potentiostat (Wuhan, China). The CV and EIS measurements utilized platinum sheets as the counter electrode, Ag/AgCl as the reference electrode, and the working electrode, with a surface area of 0.5 cm², composed of thin films and nanodots deposited on ITO glass. The solution used for CV testing was a 5.0 mM $[Fe(CN)_6]^{3-/4-}$ solution. Variations employed for CV testing included cancer cell concentrations in mixtures containing 10 µL of CCRF-CEM cells in 1×PBS, with concentrations ranging from 10^2 to 10^6 cells/mL, as determined by the TC20 Automated Cell Counter. Testing was conducted at potentials ranging from –0.4 to 0.8 V with scan rate variations (49, 64, 81, 100, 121, 144, and 169 mV/s) and performed for 10 cycles. Electrochemical testing was carried out at room temperature (30 ± 2 °C). Testing using BSA, glucose, urea, and glycerol in 1×PBS was also conducted to determine electrode selectivity.

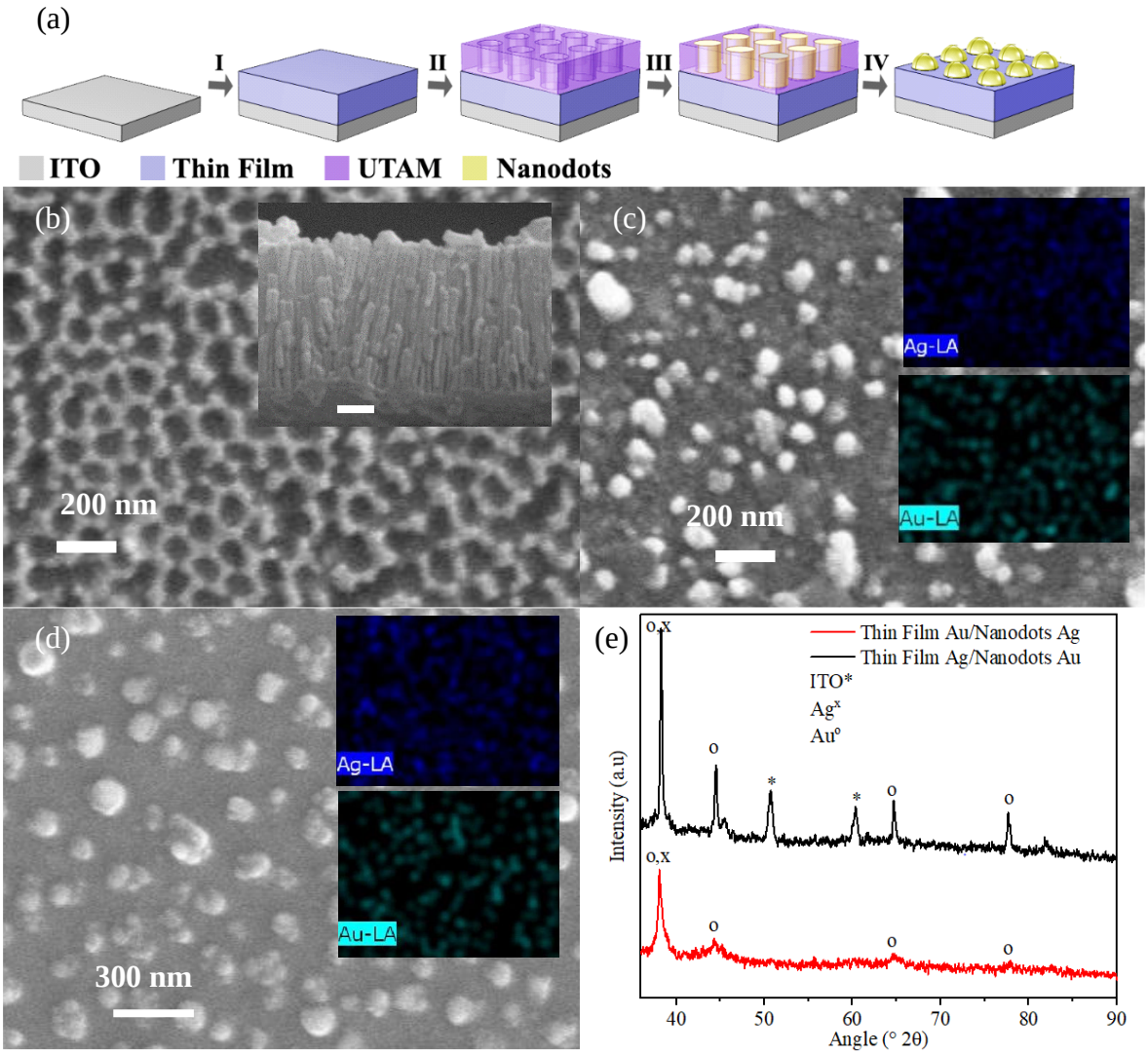

Figure 1: (a) Illustration of the diagram for making of thin films/nanodots, (b) SEM results on top view section and side insert, view section of UTAM, SEM and EDX test results of the arrangement of (c) an Au thin film/Ag nanodots and (d) an Ag thin film/ Au nanodots, and (e) XRD test results of an Au thin film/Ag nanodots and an Ag thin film/Au nanodots.

2.7 *Simulation of a binding molecule*

This study employs various molecules. The crystal structure of tyrosine kinase 2 JH2 (pseudokinase domain) with protein data bank (PDB) ID 7K7O was acting as a protein bioreceptor. The human carbonic anhydrase II complexed with urea with PDB ID 1BV3, the crystal structure of bovine serum albumin with PDB ID 3V03, and 3D structure databases of glucose and glycerol were acting as target molecules to simulate intermolecular bonds [19]–[23]. Each molecule's data in the PDB file format will be uploaded to the ClusPro page, and the resulting bond and binding energy models will be obtained for further analysis [24].

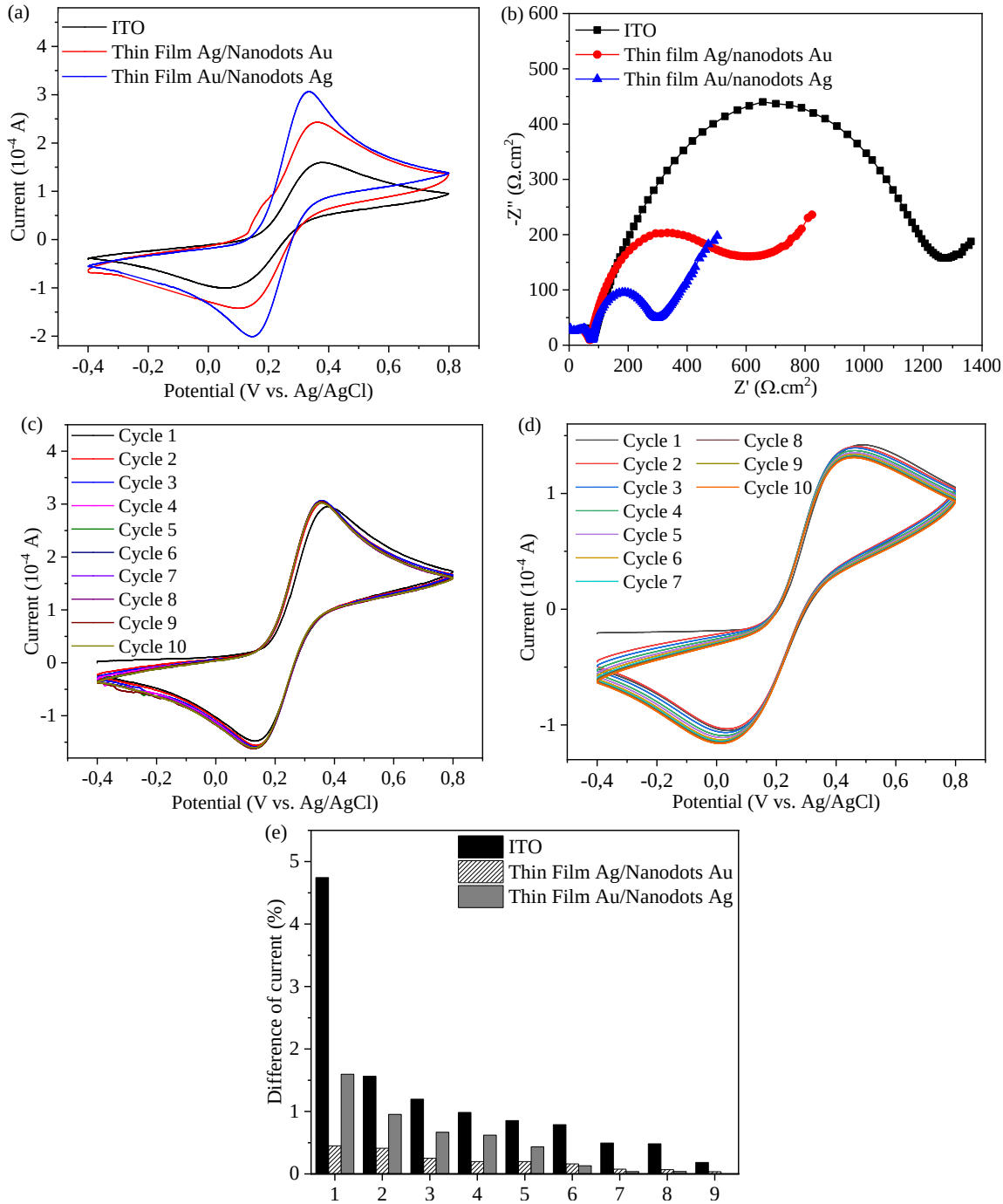

Figure 2: (a) CV and (b) EIS test results of ITO, the arrangement of an Au thin film/Ag nanodots and an Ag thin film/ Au nanodots. Test results 10 cycles of CV of (c) Au Thin Film/Ag nanodots and (d) Au Thin Film/Ag nanodots. (e) The difference in the value of the oxidation current compared to the previous cycle using 10 cycles of testing on ITO, Au thin film/Ag nanodots and Ag thin film/Au nanodots.

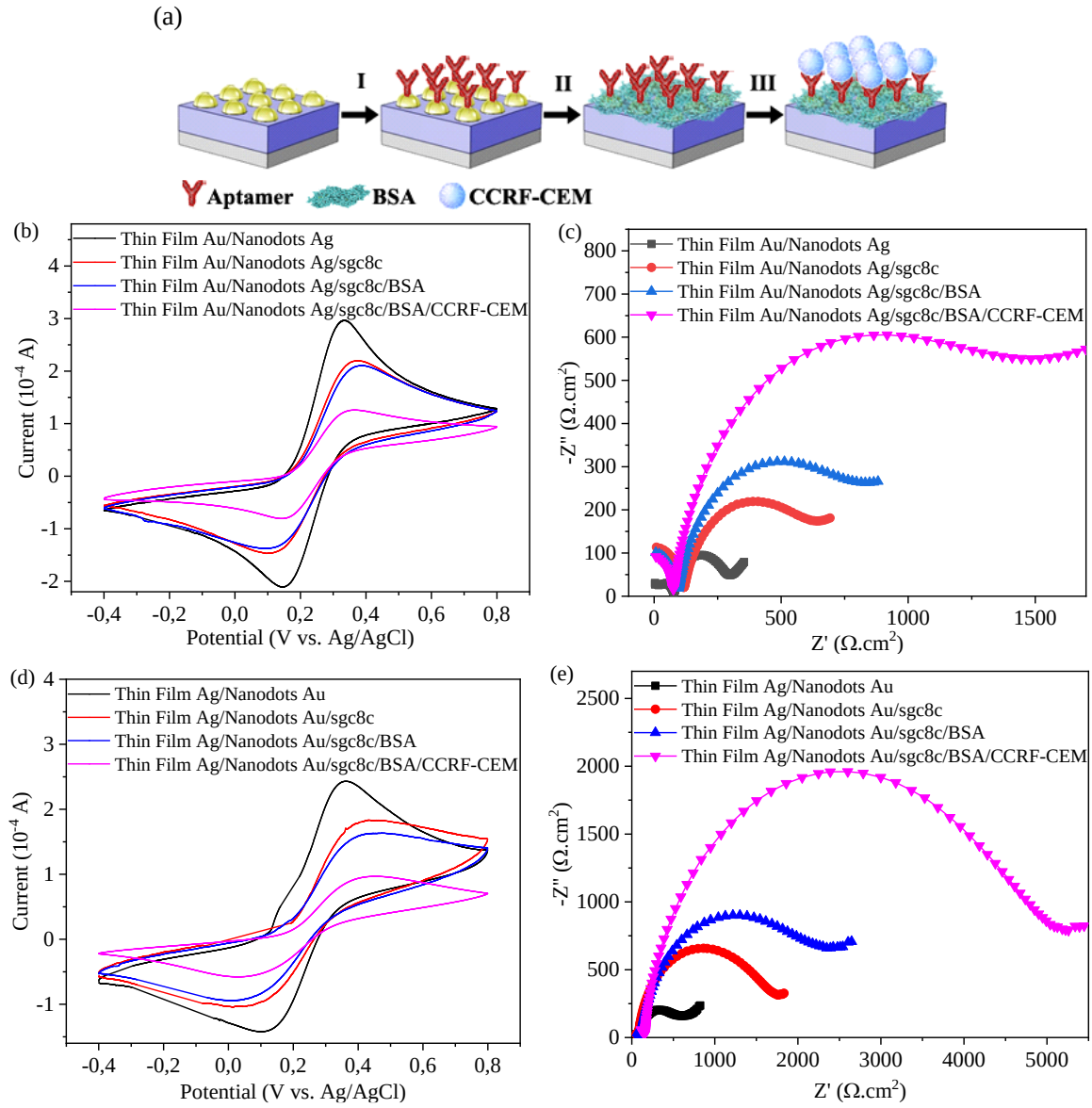

Figure 3: (a) Illustration of Electrode Surface Preparation and test results (b) CV and (c) EIS analysis with varying surface preparations on Au thin films/Ag nanodots; (d) CV and (e) EIS analysis with varying surface preparations on Ag thin films/Au nanodots at a CCRF-CEM cell concentration of 10^6 cells/mL.

3 Results and Discussion

3.1 *Morphological characterization and microstructural analysis*

The fabrication process involves thin layer deposition, transferring of UTAM to the substrate, nanodot deposition, and UTAM release to create a thin film/nanodot electrode configuration (Figure 1(a)). The resulting UTAM template has a diameter of 170 nm and a depth of 1.5 µm, with a spacing of 20 nm between the pores. UTAM samples, attached to ITO coated with thin films, were coated with Au and Ag, resulting in configurations of Ag thin film/Au nanodots and Au thin film/Ag nanodots upon UTAM removal. SEM and EDX testing of these electrodes

(Figure 1(c) and (d)) reveal nanodot sizes of 165.51±7.15 nm adhering to the thin film, with even deposition of Au and Ag particles confirmed. The resulting nanodots are evenly spread, with a distance range of 99.07±8.23 nm. The EDX results show that for Au thin films/Ag nanodots, the weight percentages of Ag and Au are 18% and 30%, respectively. In contrast, for Ag thin films/Au nanodots, the weight percentages of Ag and Au are 41% and 42%, respectively. Figure 1e shows XRD patterns of the electrodes, revealing indicating the crystalline phase. Although the Ag thin film/Au nanodot electrode exhibits the highest crystallinity, both configurations are suitable for iosensor applications due to their crystalline structures [25]. The presence of Ag and Au results in new phases with face-centered cubic structures, with side lengths of 4.15 Å and 4.09 Å, respectively. Ag deposition shows crystalline phases with Miller indices of (111), (002), and (022), while Au deposition displays diffraction peaks with Miller indices of (111), (002), (022), and (113) [26] distinct diffraction pattern peaks.

3.2 *Electrochemical analysis of the electrodes and surface modification*

Assessing biosensor materials like ITO, Ag thin film/Au nanodots, and Au thin film/Ag nanodots involves evaluating their reversibility using CV, as shown in Figure 2(a). ITO shows moderate reversibility, while Ag thin film/Au nanodots exhibit good, and Au thin film/Ag nanodots display high reversibility. A smaller separation between oxidation and reduction peaks indicates higher reversibility. Additionally, EIS measurements, depicted in Figure 2(b), reveal that Au thin film/Ag nanodots have low solution resistance (Rs: 68.932 Ω), high capacitance (C: 3.78×10^{-6} F), and small charge transfer resistance (Rp: 262.24 Ω), indicating its potential as a biosensor material [27], [28]. These findings highlight Au thin film/Ag nanodots efficiency in electron transfer kinetics, suggesting improved sensitivity and accuracy in biosensors, making it a promising candidate for further development.

The CV data, particularly the percentage difference in oxidation current over 10 cycles, offers insights into the reproducibility capabilities of different electrode materials, as shown in Figure 2(c) and (d). In biosensors, precision and consistency are crucial, making understanding electrode reproducibility significant. ITO initially exhibits the highest percentage difference in oxidation current (4.741%), which gradually diminishes over cycles, indicating a stabilization of the electrode over time. In contrast, both Ag thin film/Au nanodots and Au thin film/Ag nanodot electrodes start with lower initial percentage differences, showing better reproducibility from the outset. With continued cycling, these materials consistently display decreasing percentage differences, suggesting enhanced stability and reproducibility over time [29]. Incorporating thin film and nanodots of silver and gold can initially improve reproducibility characteristics [30].

In this research, the biosensor is tailored for the specific identification of CCRF-CEM cells. The surface of the electrode underwent a sequential modification process as shown in Figure 3(a), starting with the deposition of a thin film and nanodots. Subsequently, the aptamer sgc8c was immobilized onto the surface of nanodots. Sgc8c has the ability to capture probes, which specifically recognize PTK7 on the target cell membrane of CCRF-CEM cells [31]. To minimize non-specific interactions, BSA was effectively blocking inactive and unspecified binding sites [32]. The effects of these surface modifications were assessed through CV and EIS measurements conducted on the Au thin film/Ag nanodots electrode, illustrated in Figure 3(b) and (c). Upon immobilization of sgc8c, a notable reduction in the maximum oxidation current from 2.969×10^{-4} A to 2.199×10^{-4} A was observed in CV, indicating successful binding of the aptamer to the electrode surface [33], [34]. Concurrently, in EIS measurements, there was a noticeable increase in capacitance from 3.78×10^{-6} F to 5.80×10^{-6} F, confirming the successful immobilization of sgc8c and highlighting its specificity for target cell recognition. Subsequent introduction of BSA further decreased the current in CV to 2.105×10^{-6} A and increased capacitance to 6.05×10^{-6} F in EIS, confirming effective blocking of non-specific binding sites. Additionally, the charge transfer resistance (Rp) increased from 262.24 Ω to 504.93 Ω, indicating a reduction in the electron transfer rate due to the presence of the aptamer and BSA. Finally, upon exposure to CCRF-CEM cells, a significant decrease in the maximum oxidation current to 1.258×10^{-4} A was observed in CV, demonstrating successful and specific detection of these cells. In EIS measurements, while capacitance increased slightly to 6.10×10^{-6} F, indicating minor changes in surface properties, charge transfer resistance significantly increased to 1441.8 Ω, suggesting substantial hindrance to electron transfer due to the presence of CCRF-CEM cells [35], [36].

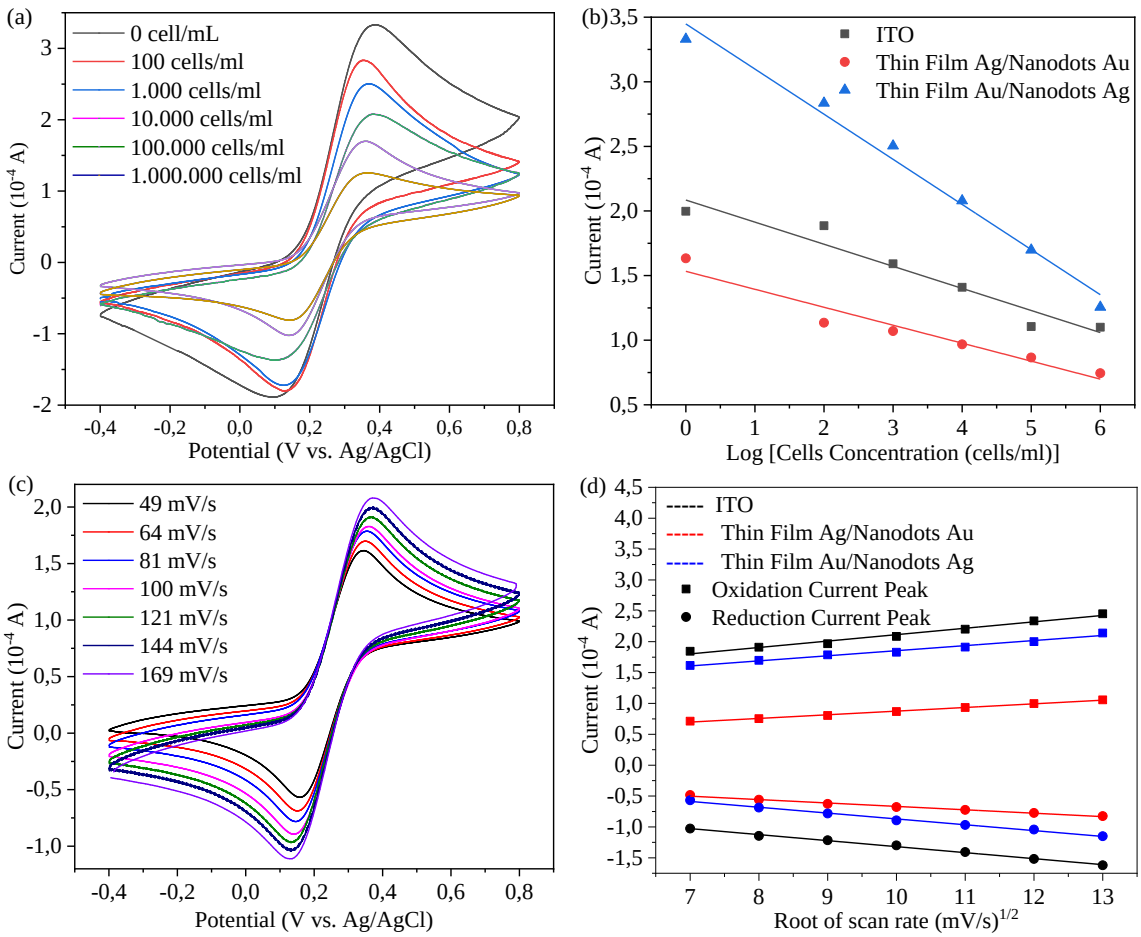

Figure 4: (a) CV of Au thin films/Ag nanodots across cell concentrations ranging from 10^2 to 10^6 cells/mL, and (b) analysis of oxidation peaks in ITO, along with the arrangement of Au thin films/Ag nanodots and Ag thin films/Au nanodots, with variations in CCRF-CEM cell concentrations from 10^2 to 10^6 cells/mL. (c) CV of Au thin films/Ag nanodots at different scan rates and (d) analysis of oxidation and reduction peaks in ITO, Au thin films/Ag nanodots, and Ag thin films/Au nanodots with varying scan rates.

3.3 *Electrochemical sensing of CCRF-CEM*

The reduction in current with increasing cell concentration (Figure 4(a)) can be attributed to several factors. As cell concentration rises, the likelihood of cell aggregation on the electrode surface increases, hindering mass transport of electroactive species and diminishing overall current response [37], [38]. Higher cell concentrations may also lead to electrode surface fouling by cellular debris or biomolecules, further impeding electron transfer kinetics and attenuating current signals [39], [40]. These combined effects contribute to the understanding of underlying electrochemical processes for accurate biosensor interpretation. The analysis detailed in Figure 4(b) provides insights into performance differences among ITO, Ag thin film/Au nanodots, and Au thin film/Ag nanodots electrodes during CV analysis across a logarithmic range of CCRF-CEM cell concentrations. Variations in current response patterns highlight nuanced differences in electrode sensitivity. The CV measurements reveal complex responses from the Ag thin film/Au nanodots and Au thin film/Ag nanodots. Notably, the Au thin film/Ag nanodots consistently record the highest oxidation current, particularly at lower cell concentrations, indicating high sensitivity as shown in Figure 4(b) and Figure S1. Ag thin film/Au nanodots display intermediate current values.

Additionally, LOD values enrich the discourse, with Au thin film/Ag nanodots showing superior detection capabilities (LOD: 16 cell/10 mL) compared to Ag thin film/Au nanodots (LOD: 26 cells/10 mL) and ITO (LOD: 27 cells/10 mL) electrodes. This emphasizes the crucial role of electrode structure and material selection in optimizing biosensor performance for detecting low cell concentrations [41], [42]. The substantially lower LOD associated with Au thin film/Ag nanodots not only underscores its height and sensitivity but also positions it as the preferred choice for biosensing applications necessitating precise detection, even at challenging concentration levels.

Cyclic voltammograms (CVs) were recorded across scan rates from 49 mV/s to 169 mV/s (Figure 4(c) and (d)) to examine electrochemical characteristics crucial for effective cell detection in biosensors. Analysis using the Randles-Sevcik equation as shown in Equation S1 revealed a direct correlation between peak current (I_p) and the square root of the scan rate ($v^{1/2}$), indicating diffusion-controlled processes [43]. Linear regression analysis showed exceptional performance of the ITO electrode with a high adjusted R-square value of 0.99483 for reduction peak current, indicating significant sensitivity and consistent reaction kinetics across different scan rates. Ag thin films/Au nanodots and Au thin film/Ag nanodots exhibited elevated adjusted R-square values of 0.99475 and 0.99392, respectively, suggesting sensitivity to scan rate changes and rapid electron transfer rates, desirable for biosensor applications [44].

The scan rate-dependent behavior of peak currents suggests that the ITO electrode promotes faster electrochemical reactions, while electrodes modified with silver and gold nanodots exhibit somewhat slower kinetic responses [45], [46]. These findings emphasize the sensitivity and kinetic advantages of the ITO electrode and highlight the need for further exploration into the electron transfer kinetics of nanodot-modified electrodes. Understanding the nuanced kinetics of each electrode material is crucial for biosensor design and application, directly influencing the sensor's capacity to swiftly and accurately detect changes in cellular concentrations. Calibration against variations in scan rate and interpretation of kinetic data establish a sturdy groundwork for the biosensor's deployment in clinical diagnostics, environmental monitoring, and other fields, ensuring reliable performance in swiftly detecting cells within complex biological samples.

Serum albumin, glucose, urea, and glycerol are essential components found in blood, each serving distinct physiological roles. Serum albumin maintains osmotic pressure and transports hormones, fatty acids, and drugs throughout the body, crucial for fluid balance and tissue integrity. Normal serum albumin levels typically range from 3.5 to 5.0 g/dL [47]. Glucose, derived from dietary carbohydrates and glycogen stores, provides primary energy for cellular functions, with normal fasting levels ranging from 70-100 mg/dL [48]. Urea, a byproduct of protein metabolism, reflects renal function and is typically present in blood at levels of 8–16 mg/dL [49]. Glycerol, originating from triglyceride breakdown, aids in energy metabolism and liver gluconeogenesis, with concentrations in blood around 0.5–1 mg/dL [50]. These compounds' presence and regulation in the bloodstream are crucial for maintaining homeostasis and supporting vital metabolic processes throughout the body.

Figure 5(a) oxidation peak values from CV measurements offer insight into the selectivity of various binding targets using essential components found in blood. Exposing the Sgc8c aptamer to a mixture of CCRF-CEM cells a concentration of 10^6 cells/mL and other blood substances showed consistently decreased oxidation peak values for the sgc8c/CCRF-CEM complex, indicating the aptamer's specificity for CCRF-CEM cells with minimal interference from non-target molecules. The oxidation peak value for the sgc8c/CCRF-CEM complex had the consistently highest decrease, i.e., 1.15×10^{-4} A, comparable to that observed for the aptamer alone and other control substances (serum albumin, glucose, urea, and glycerol). Each electrode type's selectivity in detecting CCRF-CEM cells with the aptamer Sgc8c was evaluated based on current discrepancies. The Ag thin film/Au nanodot electrode displayed the highest selectivity, with a significant current increase compared to other samples, showing a deviation of 58.94%. The ITO electrode also demonstrated selectivity, albeit to a lesser degree (deviation of 15.87%). The Au thin film/Ag nanodot electrode showed selectivity as well, though inferior to the other two electrodes (deviation of 42.77%). These findings underscore the critical role of electrode choice in biosensor design, with the Ag thin film/Au nanodots electrode emerging as the most promising option for precise CCRF-CEM cell detection using the aptamer Sgc8c.

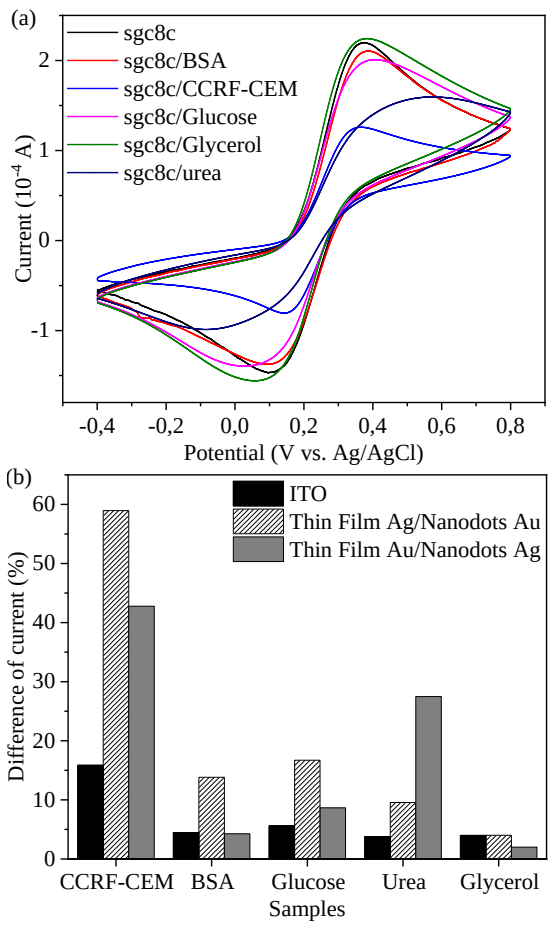

Figure 5: Test results (a) CV of Au thin films/Ag nanodots and (b) analysis of oxidation peaks in ITO, arrangements of Au thin films/Ag nanodots and Ag thin films/Au nanodots with various analytes.

3.4 *Binding molecule simulation*

To delve deeper into the molecular interactions dictating this selectivity, an examination was conducted on the binding energies between the protein bioreceptor and each molecule (Figure S2). An examination of binding energies between the protein bioreceptor and various molecules revealed significant differences, notably a high binding energy of –877.1 kcal/mol with PTK7, a receptor on CCRF-CEM cells. In contrast, interactions with BSA (–713.8 kcal/mol), urea (–776.4 kcal/mol), glucose (–4.1 kcal/mol), and glycerol (–1.6 kcal/mol) showed lower binding energies. This underscores the protein bioreceptor's strong specificity for its target cells, enhancing the potential of electrochemical biosensors using aptamers for precise detection. Building on prior research by Albright *et al*., the study corroborates the tendency of the sgc8c aptamer to primarily bind to specific sites on PTK7, notably strands 8, 27, and 30 of sgc8c [51]. Additionally, investigations into the interaction between the sgc8c DNA aptamer and the PTK7 receptor on Jurkat T cell lymphoma membranes unveiled the formation of a stable ligand-receptor complex. Employing TREC (Topography and Recognition Imaging with AFM) techniques facilitated precise mapping of the aptamer-recognized PTK7 receptor, showcasing their potential utility as diagnostic and targeting tools for acute lymphoblastic leukemia [52].

3.5 *Comparison of electrochemical biosensor test results for detection of ALL type leukemia*

In the context of cell detection biosensors, the choice between using silver as the substrate and gold as the surface modification (self-assembled monolayers or SAMs) or gold as the substrate with silver surface modification depends on several factors, including the biosensing application, target cells, and specific requirements. ITO/gold substrates excel over ITO/silver substrates in electrochemical biosensors due to gold's superior stability, biocompatibility, reduced interference, and long-term reliability. The study by Aiemderm *et al*., demonstrates that electro-deposited gold (Au) surfaces on carbon electrodes are highly suitable for constructing immunosensors for use in human serum. SPCE/Au electrodes exhibited significantly higher peak currents compared to SPCE/GO, especially in serum, indicating superior sensitivity. Additionally, Au-modified electrodes showed lower baseline slopes and reduced non-specific protein adsorption, enhancing measurement accuracy and specificity. The stability, high surface-to-volume ratio, and excellent electroconductivity of Au facilitate the stable immobilization of biomolecules [53].

Silver substrate with gold SAMs provides specific binding due to gold's affinity for biomolecules like antibodies or DNA probes, enhancing selectivity. For the surface modification, silver's high. conductivity promotes efficient electron transfer, contributing to robust sensor performance [15]–[17]. The principle of aptamer immobilization on silver and gold biosensors can be achieved through various methods such as direct adsorption and electrostatic interactions. The negatively charged phosphate backbone of DNA aptamers interacts with positively

charged metal surfaces, which can be modified to enhance binding [54]. Moreover, ion-polar interactions play a critical role in the binding of aptamers with silver (Ag^+) and gold (Au^{3+}) ions, enhancing the stability, sensitivity, and specificity of aptamer-based sensors. These interactions occur between the metal ions and the polar regions of the aptamers, involving electrostatic attractions and specific affinities with nucleobases. Silver ions typically coordinate with thymine bases, forming stable C-Ag^+-C complexes that induce conformational changes in the aptamer, enhancing target binding with high affinity. Gold ions interact with the negatively charged phosphate backbone and nucleobases of the aptamers, with a binding affinity order of G > C > A > T, demonstrating strong binding strength, especially with guanine, which has the highest affinity for gold [55]–[57]. Adsorption relies on non-covalent interactions, while covalent bonding can be achieved using functional groups like carboxyl or amine. Gold nanoparticles (AuNPs) enhance immobilization and sensing capabilities, facilitating the attachment of aptamers through both adsorption and covalent bonding [56].

A comparative analysis between this paper and previous ones highlights significant advancements in sensitivity for detecting CCRF-CEM cells, as shown in Table 1. This paper achieved a remarkable sensitivity of 16 cells/10 mL, a substantial improvement over the previous best sensitivity of 3 to 4 cells/mL (Table 1).

This enhancement underscores the efficacy of these novel nanomaterial platforms in conjunction with the sgc8c aptamer for achieving heightened sensitivity in cell detection. It hold promise for more accurate biosensing applications, impacting fields like biomedical research and clinical diagnostics.

Apart from having the potential as a detection electrode using electrochemical methods, the simulation of electromagnetic waves on the resulting electrode also produces significant differences for the Au thin film/Ag nanodots electrode arrangement as shown in Figure S3. The difference in the peak transmittance value on the Au thin film/Ag nanodots electrode is caused by the bond that occurs between the electrode and the related biomolecules, thereby changing the refractive index value of the system [40]. This proves that optical analysis for the resulting electrode can be applied for the detection of leukemia cells on the electrode.

Table 1: Comparison of electrochemical biosensor test results for detection of ALL type leukemia literature.

Detection Target	Bioreceptor	Nanomaterial Type	LOD	Linear Detection Range	Ref.
Leukemic T	pTTBA	AuNP	0.6 ± 0.1 nM	0.7 nM – 1500 μM	[58]
CCRF-CEM	sgc8c aptamer	$AgInS_2$	16 cells/mL	150–3.0 × 10^5 cells/mL	[59]
DNA target	catechol	AuNP	1 pM	100.0 μM –10.0 pM	[60]
HL 60	Aptamer KH1C12	AuNP	250 cells/mL	25–5 × 10^5 cells mL^{-1}	[11]
CCRF-CEM	PTCA/aptamer	MWCNTs, Pd_{nano}	8 cells/mL	10–5.0×10^5 cells/mL	[61]
CCRF-CEM	Sgc8c aptamer	ZnO nanodisk@g-C_3N_4 QDs	20 cell/mL	20–20,000 cell/mL	[31]
HL 60	KH1C12	AuNP	4 cells/ 10 mL	500–7.5 × 10^7 cells/mL	[62]
CCRF-CEM	sgc8c aptamer	AuNP	3.4 cells/mL	5–500 cells/mL	[63]
CCRF-CEM	sgc8c aptamer	Ag thin film/Au nanodots	26 cells/ 10 mL	10^2–10^6 cells/mL	This study
CCRF-CEM	sgc8c aptamer	Au thin film/Ag nanodots	16 cells/ 10 mL	10^2 to 10^6 cells/mL	This study

3.6 *Potential use of leukemia biosensor devices*

The leukemia detection device, employing electrochemical sensing with aptamers, shows potential as a transformative tool in medical diagnostics, alike glucose detection devices [9]. By selectively recognizing leukemic cells through aptamer-based binding on a modified electrode surface, it offers a paradigm shift in leukemia detection. Much like glucose detection devices, which rely on electrochemical reactions triggered by glucose-enzyme interactions, the leukemia detection device utilizes electrochemical sensing to capture alterations in the electrode's properties induced by leukemic cell-aptamer interactions, reflecting leukemic cell presence and its concentration in blood samples [64]. Despite blood sample complexity, specificity provided by aptamer sgc8c ensures targeted leukemic cell capture. Research using CCRF-CEM cells obtained linear detection ranges from 10^2 to 10^6 cells/ml, aligning with blast cell concentration limits for ALL sufferers [65]. Electrodes with low LOD enable early ALL detection based on lymphoblast concentration in blood. Shared utilization of electrochemical principles underscores the efficacy of electrochemical sensing in medical diagnostics, with the leukemia detection device offering insights into disease characteristics and progression akin to glucose detection devices in diabetes management.

4 Conclusions

In this paper, a specialized biosensor meticulously developed for the precise detection of CCRF-CEM cells has been introduced, achieved through a combination of advanced surface modification techniques and sophisticated electrochemical analysis. The fabrication process involved intricate procedures including electropolishing, dual anodization, and pore widening, ensuring the creation of a uniformly structured AAO template. Through the utilization of DC sputtering deposition techniques, nanostructured electrodes with compositions such as Ag thin film/Au nanodots and Au thin film/Ag nanodots were synthesized. The conversion of AAO into UTAM facilitated precise electrode patterning, leading to the identification of the Au thin film/Ag nanodots electrode as the most promising candidate for CCRF-CEM detection. This electrode exhibited exceptional sensitivity, with a low LOD of 16 cells/10 mL and consistent peak oxidation currents, it demonstrated remarkable reproducibility, with a minimal percentage difference in oxidation current (<5%) over multiple cycles, ensuring robust performance under diverse conditions. Moreover, the electrode displayed notable selectivity for CCRF-CEM cells. Its impressive features suggest it could greatly enhance biosensor tech for disease detection. This paper stresses the need for advanced fabrication and characterization methods to create efficient biosensors for specific medical uses. Using a method targeting leukemic cells with aptamer-based binding, this research offers a breakthrough in leukemia detection, akin to glucose monitors. Overall, it's a big step forward in biosensor tech, offering innovative ways to detect and monitor diseases in clinics.

Acknowledgments

The authors are grateful for the financial support from the Institut Teknologi Sepuluh Nopember under the project scheme of BRIN on RIIM batch 4 awards number: 37/II.7/HK/2023.

Author Contributions

U.F.: conceptualization, methodology, software, validation, investigation, data curation, writing an original draft, and visualization; M.F.: visualization; P.W.: methodology, and project administration conceptualization; I.A.: validation, and formal analysis; H.S.: resources and visualization; N.J.: supervision; R.K.U.: funding acquisition; A.R.: conceptualization, writing—reviewing and editing, supervision, and project administration; N.N.: conceptualization, validation, investigation, writing an original draft, supervision, and funding acquisition. All authors have read and agreed to the published version of the manuscript.

Conflicts of Interest

The authors declare no conflict of interest.

References

[1] M. Abramovitz, *Leukemia*. New York: Greenhaven Publishing, 2010.

[2] The Leukemia & Lymphoma Society, "Facts: Updated Data on Blood Cancers | Leukemia and Lymphoma Society," 2023. [Online]. Available: https://www.lls.org/booklet/facts-updated-data-blood-cancers

[3] American Cancer Society, "Cancer Facts and Statistics," 2023. [Online]. Available: https://www.cancer.org/research/cancer-facts-statistics.html

[4] M. P. Coleman, M. Quaresma, F. Berrino, J. M. Lutz, R. De Angelis, R. Capocaccia, P. Baili, B. Rachet, G. Gatta, T. Hakulinen, A. Micheli, M. Sant, H. K. Weir, J. M. Elwood, H. Tsukuma, S. Koifman, G. A. E. Silva, S. Francisci, M. Santaquilani, A. Verdecchia, H. H. Storm, J. L. Young, "Cancer survival in five continents: A worldwide population-based study (CONCORD)," *The Lancet Oncology*, vol. 9, no. 8, pp. 730–756, 2008, doi: 10.1016/S1470-2045(08)70179-7.

[5] J. Song, H.-J. Kim, C. Lee, S. J. Kim, S. Hwang, and T. S. Kim, "Identification of gene expression signatures for molecular classification in human leukemia cells," *International Journal of Oncology*, vol. 29, no. 1, pp. 57–64, 2006, doi: 10.3892/IJO.29.1.57.

[6] T. Lightfoot and E. Roman, "Causes of childhood leukaemia and lymphoma," *Toxicology and Applied Pharmacology*, vol. 199, no. 2, pp. 104–117, 2004, doi: 10.1016/J.TAAP.2003.12.032.

[7] P. Dörge, B. Meissner, M. Zimmermann, A. Möricke, A. Schrauder, J. P. Bouquin, D. Schewe, J. Harbott, A. T. Schlegel, R. Ratei, W. D. Ludwig, R. Koehler, C. R. Bartram, M. Schrappe, M. Stanulla, and G. Cario, "IKZF1 deletion is an independent predictor of outcome in pediatric acute lymphoblastic leukemia treated according to the ALL-BFM 2000 protocol,"

Haematologica, vol. 98, pp. 428–432, 2010, doi: 10.3324/haematol.2011.056135.

[8] P. Das, V. A. Diya, S. Meher, R. Panda, and A. Abraham, "A systematic review on recent advancements in deep and machine learning based detection and classification of acute lymphoblastic leukemia," *IEEE Access*, vol. 10, pp. 81741–81763, 2022, doi: 10.1109/access.2022.3196037.

[9] U. Farahdina, T. Amrillah, M. Mashuri, V. Lee, and N. Nasori, "A novel nanobiosensor for electrochemical and optical diagnosis of leukemia: challenge and opportunity," *Journal of Innovative Optical Health Sciences*, vol. 17, no. 04, 2024, Art. no. 2430003, doi: 10.1142/S1793545824300039.

[10] J. Wang, "Electrochemical biosensors: Towards point-of-care cancer diagnostics," *Biosensors & Bioelectronics*, vol. 21, no. 10, pp. 1887–1892, 2006, doi: 10.1016/J.BIOS.2005.10.027.

[11] M. A. Tabrizi, M. Shamsipur, R. Saber, and S. Sarkar, "Isolation of HL-60 cancer cells from the human serum sample using MnO_2-PEI/Ni/Au/aptamer as a novel nanomotor and electrochemical determination of thereof by aptamer/gold nanoparticles-poly(3,4-ethylene dioxythiophene) modified GC electrode," *Biosensors and Bioelectronics*, vol. 110, pp. 141–146, 2018, doi: 10.1016/j.bios.2018.03.034.

[12] Y. Sun, Q. Ren, B. Liu, Y. Qin, and S. Zhao, "Enzyme-free and sensitive electrochemical determination of the FLT3 gene based on a dual signal amplified strategy: Controlled nanomaterial multilayers and a target-catalyzed hairpin assembly," *Biosensors and Bioelectronics*, vol. 78, pp. 7–13, 2016, doi: 10.1016/j.bios.2015.11.014.

[13] T. Hianik, "Advances in electrochemical and acoustic aptamer-based biosensors and immunosensors in diagnostics of leukemia," *Biosensors*, vol. 11, no. 6, pp. 177, 2021, doi: 10.3390/bios11060177.

[14] A. Malysheva, A. Ivask, C. L. Doolette, N. H. Voelcker, and E. Lombi, "Cellular binding, uptake and biotransformation of silver nanoparticles in human T lymphocytes," *Nature Nanotechnology*, vol. 16, no. 8, pp. 926–932, 2021, doi: 10.1038/s41565-021-00914-3.

[15] C. Salvo-Comino, F. Martín-Pedrosa, C. García-Cabezón, and M. L. Rodriguez-Mendez, "Silver nanowires as electron transfer mediators in electrochemical catechol biosensors," *Sensors*, vol. 21, no. 3, p. 899, 2021, doi: 10.3390/s21030899.

[16] Y. Liu, D. Zhang, E. Alocilja, and S. Chakrabartty, "Biomolecules detection using a silver-enhanced gold nanoparticle-based biochip," *Nanoscale Research Letters*, vol. 5, pp. 533–538, 2010, doi: 10.1007/s11671-010-9542-0.

[17] X. Ren, X. Meng, D. Chen, F. Tang, and J. Jiao, "Using silver nanoparticle to enhance current response of biosensor," *Biosensors & Bioelectronics*, vol. 21 3, pp. 433–7, 2005, doi: 10.1016/J.BIOS.2004.08.052.

[18] D. V. Sotnikov, A. N. Berlina, V. S. Ivanov, A. V. Zherdev, and B. B. Dzantiev, "Adsorption of proteins on gold nanoparticles: One or more layers?," *Colloids and Surfaces B: Biointerfaces*, vol. 173, pp. 557–563, 2019, doi: 10.1016/j.colsurfb.2018.10.025.

[19] PubChem, "Glycerin," 2024. [Online]. Available: https://pubchem.ncbi.nlm.nih.gov/compound/753

[20] A. Rutz, J. Bisson, and P.-M. Allard, "The LOTUS initiative for open natural products research: Frozen dataset union wikidata (with metadata)," 2023, doi: 10.5281/zenodo.5794106.

[21] C. Liu, J. Lin, C. Langevine, D. Smith, J. Li, J. S. Tokarski, J. Khan, M. Ruzanov, J. Strnad, A. Z. Fernandez, L. Cheng, K. M. Gillooly, D. Shuster, Y. Zhang, A. Thankappan, K. W. McIntyre, C. Chaudhry, P. A. Elzinga, M. Chiney, A. Chimalakonda, L. J. Lombardo, J. E. Macor, P. H. Carter, J. R. Burke, and D. S. Weinstein, "Discovery of BMS-986202: A clinical Tyk2 inhibitor that binds to Tyk2 JH2," *Journal of Medicinal Chemistry*, vol. 64, no. 1, pp. 677–694, 2021, doi: 10.1021/acs.jmedchem.0c01698.

[22] F. Briganti, S. Mangani, A. Scozzafava, G. Vernaglione, and C. T. Supuran, "Carbonic anhydrase catalyzes cyanamide hydration to urea: Is it mimicking the physiological reaction?," *Journal of Biological Inorganic Chemistry*, vol. 4, no. 5, pp. 528–536, 1999, doi: 10.1007/s007750050375.

[23] K. A. Majorek, P. J. Porebski, A. Dayal, M. D. Zimmerman, K. Jablonska, A. J. Stewart, M. Chruszcz, and W. Minor, "Structural and immunologic characterization of bovine, horse, and rabbit serum albumins," *Molecular Immunology*, vol. 52, no. 3–4, pp. 174–182, 2012, doi: 10.1016/j.molimm.2012.05.011.

[24] D. Kozakov, D. R. Hall, B. Xia, K. A. Porter, D. Padhorny, C. Yueh, D. Beglov, and S. Vajda,

"The ClusPro web server for protein–protein docking," *Nature Protocols*, vol. 12, no. 2, pp. 255–278, 2017, doi: 10.1038/nprot.2016.169.

[25] M. A. Khan, Y. Zhu, Y. Yao, P. Zhang, A. Agrawal, and P. J. Reece, "Impact of metal crystallinity-related morphologies on the sensing performance of plasmonic nanohole arrays," *Nanoscale*, vol. 12, no. 14, pp. 7577–7585, 2020, doi: 10.1039/D0NR00619J.

[26] X. Yan, P. Lin, X. Qi, and L. Yang, "Finnis–Sinclair potentials for fcc Au–Pd and Ag–Pt alloys," *International Journal of Materials Research*, vol. 102, no. 4, pp. 381–388, 2011, doi: 10.3139/146.110488.

[27] K. Fu, J.-W. Seo, V. Kesler, N. Maganzini, B. D. Wilson, M. Eisenstein, B. Murmann, and H. T. Soh, "Accelerated electron transfer in nanostructured electrodes improves the sensitivity of electrochemical biosensors," *Advanced Science*, vol. 8, 2021, Art. no. 2102495, doi: 10.1002/advs.202102495.

[28] E. Randviir, "A cross examination of electron transfer rate constants for carbon screen-printed electrodes using electrochemical impedance spectroscopy and cyclic voltammetry," *Electrochimica Acta*, vol. 286, pp. 179–186, 2018, doi: 10.1016/J.ELECTACTA.2018.08.021.

[29] M. Yaşa, S. Surmeli, T. Depci, L. Toppare, and S. Hacioglu, "Synthesis of a multifunctional quinoxaline and benzodithiophene bearing polymer and its electrochromic device applications," *Macromolecular Chemistry and Physics*, vol. 221, 2020, Art. no. 1900470, doi: 10.1002/macp.201900470.

[30] X. Yang and Z. Gao, "Enzyme-catalysed deposition of ultrathin silver shells on gold nanorods: a universal and highly efficient signal amplification strategy for translating immunoassay into a litmus-type test," *Chemical Communications*, vol. 51, no. 32, pp. 6928–6931, 2015, doi: 10.1039/c5cc01286d.

[31] X. Pang, C. Cui, M. Su, Y. Wang, Q. Wei, and W. Tan, "Construction of self-powered cytosensing device based on ZnO nanodisks@g-C3N4 quantum dots and application in the detection of CCRF-CEM cells," *Nano Energy*, vol. 46, pp. 101–109, 2018, doi: 10.1016/j.nanoen.2018.01.018.

[32] J. Lee, I.-S. Park, H. Kim, J.-S. Woo, B.-S. Choi, and D.-H. Min, "BSA as additive: A simple strategy for practical applications of PNA in bioanalysis," *Biosensors and Bioelectronics*, vol. 69, pp. 167–173, 2015, doi: 10.1016/j.bios.2015.02.030.

[33] Y. Kim, H.-S. Jung, T. Matsuura, H.-Y. Lee, T. Kawai, and M. Gu, "Electrochemical detection of 17beta-estradiol using DNA aptamer immobilized gold electrode chip," *Biosensors & bioelectronics*, vol. 22, no. 11, pp. 2525–2531, 2007, doi: 10.1016/J.BIOS.2006.10.004.

[34] F. A. Armstrong, R. Camba, H. A. Heering, J. Hirst, L. J. C. Jeuken, A. K. Jones, C. Léger, and J. P. McEvoy, "Fast voltammetric studies of the kinetics and energetics of coupled electron-transfer reactions in proteins," *Faraday Discussions*, vol. 116, pp. 191–203, 2000, doi: 10.1039/B002290J.

[35] M. Cohen-Atiya and D. Mandler, "Studying electron transfer through alkanethiol self-assembled monolayers on a hanging mercury drop electrode using potentiometric measurements," *Physical Chemistry Chemical Physics*, vol. 8, no. 38, pp. 4405–4409, 2006, doi: 10.1039/B609560G.

[36] Y. Jin, "Label-free monitoring of site-specific DNA cleavage by EcoRI endonuclease using cyclic voltammetry and electrochemical impedance," *Analytica Chimica Acta*, vol. 634, no. 1, pp. 44–48, 2009, doi: 10.1016/j.aca.2008. 12.005.

[37] K. Kaniewska, W. Hyk, Z. Stojek, and M. Karbarz, "Diffusional and migrational transport of ionic species affected by electrostatic interactions with an oppositely charged hydrogel layer attached to an electrode surface," *Electrochemistry Communications*, vol. 88, pp. 97–100, 2018, doi: 10.1016/J.ELECOM.2018.02.004.

[38] P. St-Pierre and N. Petersen, "Relative ligand binding to small or large aggregates measured by scanning correlation spectroscopy," *Biophysical Journal*, vol. 58, no. 2, pp. 503–511, 1990, doi: 10.1016/S0006-3495(90)82395-X.

[39] S. Peng, D.-W. Liang, P. Diao, Y. Liu, F. Lan, Y. Yang, S. Lu, and Y. Xiang, "Nernst-ping-pong model for evaluating the effects of the substrate concentration and anode potential on the kinetic characteristics of bioanode," *Bioresource Technology*, vol. 136, pp. 610–616, 2013, doi: 10.1016/j.biortech.2013.03.073.

[40] U. Farahdina, A. S. Muliawati, V. Z. Zulfa, M. Firdhaus, I. Aziz, H. Suprihatin, D. Darsono, N. Nasori, and A. Rubiyanto, "Electrochemical and optical analysis of various compositions of Au and Ag layers for blood cancer prognosis,"

Coatings, vol. 13, no. 1, 2023, doi: 10.3390/coatings13010186.

[41] R. Misra, "Biosensors," *Materials Technology*, vol. 30, pp. 139–139, 2015, doi: 10.1179/b15z.00000000024.

[42] L. Soleymani, Z. Fang, E. Sargent, and S. Kelley, "Programming the detection limits of biosensors through controlled nanostructuring," *Nature Nanotechnology*, vol. 4, no. 12, pp. 844–848, 2009, doi: 10.1038/nnano.2009.276.

[43] A. H. Suroviec, "Introduction to electrochemistry," *Journal of Laboratory Chemical Education*, vol. 1, no. 3, pp. 45–48, 2013, doi: 10.5923/j.jlce.20130103.02.

[44] O. Dračka, "Theory of current elimination in linear scan voltammetry," *Journal of Electroanalytical Chemistry*, vol. 402, pp. 19–28, 1996, doi: 10.1016/0022-0728(95)04257-1.

[45] S. Tanimoto and A. Ichimura, "Discrimination of inner- and outer-sphere electrode reactions by cyclic voltammetry experiments," *Journal of Chemical Education*, vol. 90, pp. 778–781, 2013, doi: 10.1021/ED200604M.

[46] K. Aoki and N. Kato, "Analysis of the cyclic voltammograms associated with deposition or precipitation of the electrochemical product," *Journal of Electroanalytical Chemistry*, vol. 245, pp. 51–60, 1988, doi: 10.1016/0022-0728(88)80058-5.

[47] R. N. Moman, N. Gupta, and M. Varacallo, "Physiology, Albumin," 2024. [Online]. Available: http://www.ncbi.nlm.nih.gov/books/NBK459198/

[48] J. Feher, "9.4 - the endocrine pancreas and control of blood glucose," in *Quantitative Human Physiology*, J. Feher, Ed. Boston: Academic Press, 2012, pp. 799–809.

[49] A. O. Hosten, "BUN and Creatinine," in *Clinical Methods: The History, Physical, and Laboratory Examinations*, H. K. Walker, W. D. Hall, and J. W. Hurst, Eds. Boston: Butterworths, 1990.

[50] E. C. C. Lin, "Glycerol utilization and its regulation in mammals," *Annual Review of Biochemistry*, vol. 46, pp. 765–795, 1977, doi: 10.1146/annurev.bi.46.070177.004001.

[51] S. Albright, M. Cacace, Y. Tivon, and A. Deiters, "Cell surface labeling and detection of protein tyrosine kinase 7 via covalent aptamers," *Journal of the American Chemical Society*, vol. 145, no. 30, pp. 16458–16463, 2023, doi: 10.1021/jacs.3c02752.

[52] M. Leitner, A. Poturnayova, C. Lamprecht, S. Weich, M. Snejdarkova, I. Karpisova, T. Hianik, and A. Ebner, "Characterization of the specific interaction between the DNA aptamer sgc8c and protein tyrosine kinase-7 receptors at the surface of T-cells by biosensing AFM," *Analytical and Bioanalytical Chemistry*, vol. 409, pp. 2767–2776, 2017, doi: 10.1007/s00216 -017-0238-5.

[53] P. Aiemderm, K. Monkhang, S. Wongjard, K. Choowongkomon, N. Mongkoldhumrongkul Swainson, C. Prasittichai, C. Kraiya, "Advantages of electro-deposited gold on carbon electrodes for NT-proBNP immunosensor for development of heart failure test kit," *Applied Science and Engineering Progress*, vol. 17, no. 2, 2024, doi: 10.14416/j.asep.2023.10.004.

[54] S. S. Patil, V. N. Narwade, K. S. Sontakke, T. Hianik, and M. D. Shirsat, "Layer-by-layer immobilization of DNA aptamers on Ag-incorporated co-succinate metal–organic framework for Hg(II) detection," *Sensors*, vol. 24, no. 2, 2024, doi: 10.3390/s24020346.

[55] W. Guo, C. Zhang, T. Ma, X. Liu, Z. Chen, S. Li, and Y. Deng, "Advances in aptamer screening and aptasensors' detection of heavy metal ions," *Journal of Nanobiotechnology*, vol. 19, no. 1, p. 166, 2021, doi: 10.1186/s12951-021-00914-4.

[56] B. Chatterjee, N. Kalyani, A. Anand, E. Khan, S. Das, V. Bansal, A. Kumar, and T. K. Sharma, "GOLD SELEX: A novel SELEX approach for the development of high-affinity aptamers against small molecules without residual activity," *Microchimica Acta*, vol. 187, no. 11, p. 618, 2020, doi: 10.1007/s00604-020-04577-0.

[57] J. Li, H. Xi, C. Kong, Q. Liu, and Z. Chen, "'Aggregation-to-deaggregation' colorimetric signal amplification strategy for Ag^{+} detection at the femtomolar level with dark-field microscope observation," *Analytical Chemistry*, vol. 90, no. 19, pp. 11723–11727, 2018, doi: 10.1021/acs.analchem.8b03739.

[58] M. H. Akhtar, K. K. Hussain, N. G. Gurudatt, and Y.-B. Shim, "Detection of Ca^{2+}-induced acetylcholine released from leukemic T-cells using an amperometric microfluidic sensor," *Biosensors and Bioelectronics*, vol. 98, pp. 364–370, 2017, doi: 10.1016/j.bios.2017.07.003.

[59] J. Li, X. Lin, Z. Zhang, W. Tu, and Z. Dai, "Red light-driven photoelectrochemical biosensing for ultrasensitive and scatheless assay of tumor cells based on hypotoxic $AgInS_2$ nanoparticles," *Biosensors and Bioelectronics*, vol. 126, pp. 332–338, 2019, doi: 10.1016/j.bios.2018.09.096.

[60] M. Mazloum-Ardakani, B. Barazesh, A. Khoshroo, M. Moshtaghiun, and M. H. Sheikhha, "A new composite consisting of electrosynthesized conducting polymers, graphene sheets and biosynthesized gold nanoparticles for biosensing acute lymphoblastic leukemia," *Bioelectrochemistry*, vol. 121, pp. 38–45, 2018, doi: 10.1016/j.bioelechem.2017.12.010.

[61] M. A. Tabrizi, M. Shamsipur, R. Saber, and S. Sarkar, "Flow injection amperometric sandwich-type aptasensor for the determination of human leukemic lymphoblast cancer cells using MWCNTs-Pdnano/PTCA/aptamer as labeled aptamer for the signal amplification," *Analytica Chimica Acta*, vol. 985, pp. 61–68, 2017, doi: 10.1016/j.aca.2017.07.054.

[62] M. Su, L. Ge, S. Ge, N. Li, J. Yu, M. Yan, J. Huang, "Paper-based electrochemical cyto-device for sensitive detection of cancer cells and in situ anticancer drug screening," *Analytica Chimica Acta*, vol. 847, pp. 1–9, 2014, doi: 10.1016/j.aca.2014.08.013.

[63] B. Dou, L. Xu, B. Jiang, R. Yuan, and Y. Xiang, "Aptamer-functionalized and gold nanoparticle array-decorated magnetic graphene nanosheets enable multiplexed and sensitive electrochemical detection of rare circulating tumor cells in whole blood," *Analytical Chemistry*, vol. 91, no. 16, pp. 10792–10799, 2019, doi: 10.1021/acs.analchem.9b02403.

[64] S. Ismail-Hamdi, M. N. Romdane, and S. Ben Romdhane, "Comparison of a human portable blood glucose meter and automated chemistry analyser for measurement of blood glucose concentrations in healthy dogs," *Veterinary Medicine and Science*, vol. 7, no. 6, pp. 2185–2190, 2021, doi: 10.1002/vms3.594.

[65] G. Abdul-Hamid, "Classification of acute leukemia," in *Acute Leukemia - The Scientist's Perspective and Challenge*. London, UK: IntechOpen, 2011.

Supporting Information

$$I_p = 2.69 \times 10^5 \, n^{3/2} \, D^{1/2} \, v^{1/2} \, C \qquad \text{(S1)}$$

In the redox reaction, the variables are as follows: n represents the number of electrons participating, A represents the surface area of the redox reaction that occurs, C denotes the concentration of the redox species of the substance being analyzed, v stands for scan rate of the reaction, and D indicates the diffusion constant of the substance [1].

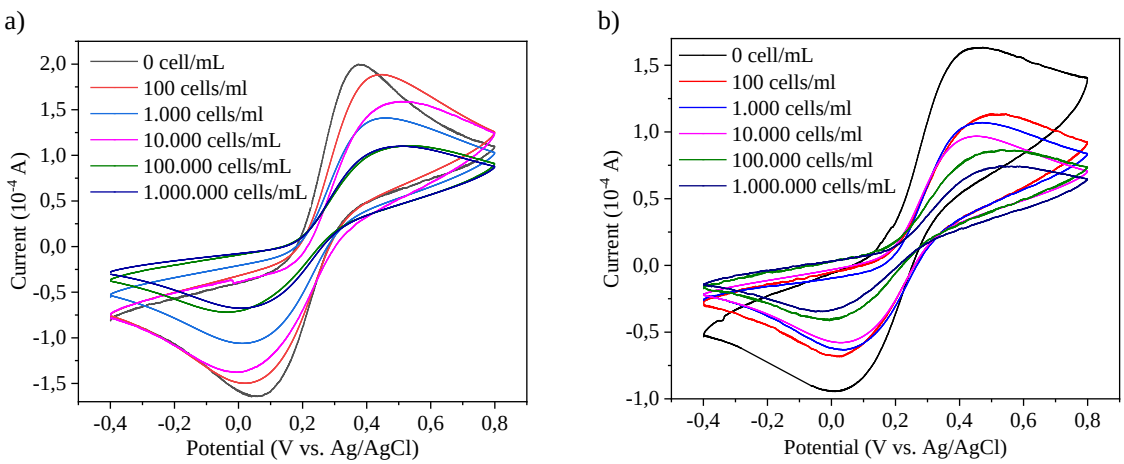

Figure S1: Test results CV using cell concentration variation of (a) ITO and (b) Ag thin films/Au nanodots.

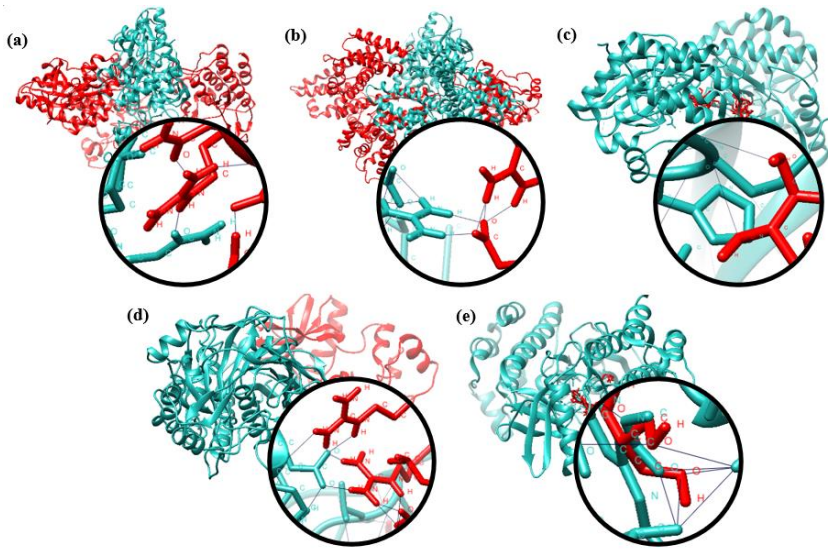

Figure S2: Illustration of molecular binding of protein bioreceptor (blue) with target molecule (red) (a) PTK7, (b) BSA, (c) glucose, (d) urea, and (e) glycerol.

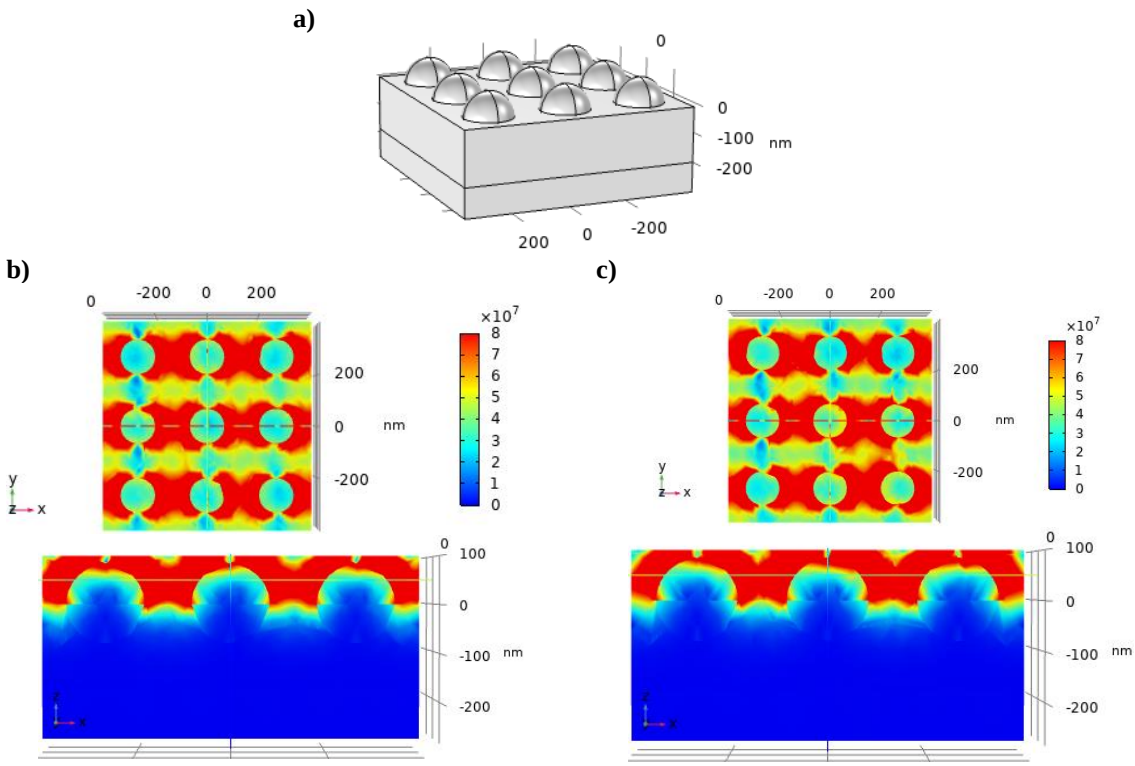

Figure S3: (a) electromagnetic wave simulation model for thin film/nanodots electrodes based on the size of thin films and nanodots measurements using SEM. Simulation results of the electric field in the top view and side view with a wavelength of 600 nm in the arrangement of (b) Au thin film/Ag nanodots/normal cells, (c) Ag thin film/Au nanodots/leukemic cells, (d) Au thin film/Ag nanodots/normal cells, and (e) Ag thin film/Au nanodots/leukemic cells. Analytical values from the transmittance simulation results were also obtained for the electrode arrangement (f) Ag thin film/ Au nanodots and (g) Au thin film/Ag nanodots.

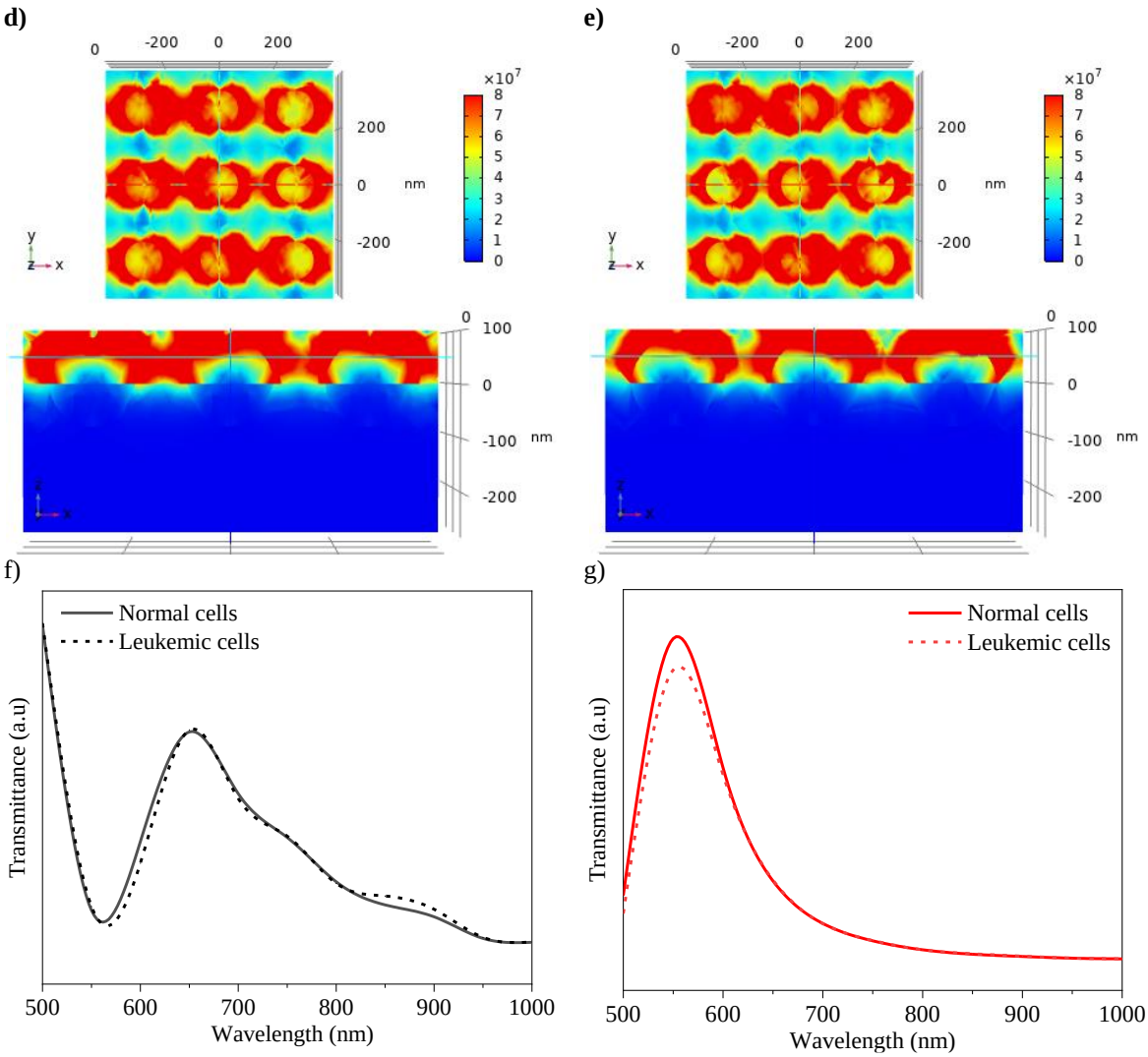

Figure S3: *Continued*.

References

[1] A. H. Suroviec, "Introduction to Electrochemistry," *Journal of Laboratory Chemical Education*, vol. 1, no. 3, pp. 45–48, 2013, doi: 10.5923/j.jlce.20130103.02.